Title
Intracellular protein delivery employing FLuc nanocapsules as a probe

Author
ZHENG, WEIBIN

Publication Date
2021

Peer reviewed|Thesis/dissertation

UNIVERSITY OF CALIFORNIA

Los Angeles

Intracellular protein delivery employing FLuc nanocapsules as a probe

A thesis submitted in partial satisfaction

of the requirements for the degree Master of Science

in Chemical Engineering

by

Weibin Zheng

2021

ABSTRACT OF THE THESIS

Intracellular protein delivery

employing FLuc nanocapsules as a probe

by

Weibin Zheng

Master of Science in Chemical Engineering

University of California, Los Angeles, 2021

Professor Yunfeng Lu, Chair

A novel protein delivery platform has been developed to efficiently deliver protein or enzyme by forming a thin polymer shell via free radical polymerization. The everlasting limitations for protein therapy are mainly poor stability and low permeability through biological barriers. The rational design of the nanocarriers based on the protein nanocapsule technology can endow nanoparticles with ideal size and reliable surface properties. In this thesis, the extent of the firefly luciferase encapsulation delivery system is further explored in the field of induced apoptosis by various drug treatments in cancer cells.

The thesis of Weibin Zheng is approved.

Samanvaya Srivastava

Junyoung O. Park

Yunfeng Lu, Committee Chair

University of California, Los Angeles

2021

Table of Contents

List of Figures

List of Tables

Acknowledgements

I would like to thank Professor Yunfeng Lu for his guidance and support in my research over the past 2 years.

I would also express my gratitude to Roxanne Castillo for her tutoring and help during all the research. Furthermore, I would give my thanks to Zheng Cao, Jie Ren and other members from the Lu lab for their constructive suggestions and continued encouragement, without which I would never deal with all this work and overcome all the obstacles.

1 Nanocapsule-based protein therapeutic delivery

1.1 Proteins for diagnostic and therapeutic purposes

As the building blocks of life, cells are the ordered assembly of molecules such as proteins and nucleic acids. These molecules regulate and participate in complex cellular processes and play different roles. For example, proteins perform biological functions, ranging from cargo transport and structural support to pathway regulation and enzymatic reactions while nucleic acids transfer information through generations. The function and the structure of proteins are continuously screened through evolution, which enables proteins to perform complex tasks specifically and efficiently. However, the malfunction of proteins can lead to pathological changes and dysfunctional cells[1]. Despite the challenges to edit the nucleic acid sequences directly and raised ethical concerns, Replacing the nonfunctional or malfunctioning proteins with new proteins delivery appears to be promising to treat diseases. It can also introduce a novel activity, protect against a toxic agent or strengthen an existing pathway[2]. Hundreds of FDA-approved therapeutic proteins are intended for various diseases since the approval of the recombinant insulin in 1982.

Proteins are required to unleash their biological functions in diseased tissues to achieve the therapeutic effect[3]. Researchers design nanocarriers and take advantage of nanotechnology for delivery purposes, which is inspired by how natural invaders such as viruses and bacteria infect human bodies with high efficiency and precision. One of the goals for biomedicine is to develop and design novel formulations for drug delivery and broaden the therapeutic potential enormously. Numerous efforts have been made in developing nanoscale delivery vehicles to advance the clinical outcome of disease management, diagnosis and monitoring.

1.2 Biological barriers to overcome for protein delivery

Various biological barriers prevent the efficient response and successful delivery of protein therapeutics after administration to patients. For example, the clearance and opsonization by the mononuclear phagocyte system (MPS) limited the drug bioavailability to target sites. In addition, endosomal escape and cellular internalization are formidable barriers. The major limitation of protein delivery can be the inability to reach therapeutic levels at the target site for protein therapeutics because of the biological barrier. The rational design of carriers is required to address these biological barriers for successful protein delivery. The details of different biological barrier are described as following.

1.2.1. Cell membrane internalization and endosomal entrapment

The plasma membrane, an elastic lipid bilayer with domains of carbohydrates, lipids and membrane proteins physically segregates the intracellular milieu form the environment[4]. Small molecules such as ions and nutrients, carbon dioxide and oxygen can be transported by specific transporters or via a free diffusion mechanism[5]. However, macromolecules like genes and proteins can be restricted by the lipophilic nature of the membranes.

The internalization is usually through the endocytic pathway, in which the internalized nanoparticles or macromolecules can be engulfed by vesicles[6]. The vesicles, formed by the cell membrane, would mature into lysosome and late endosome[7]. Massive proteases could deteriorate protein functions and digest them into small pieces. In addition, the exocytosis pathway removes the proteins into the extracellular area[8].

1.2.2. Mononuclear phagocytic system clearance

In reticular connective tissue, the phagocytic cells constitute the mononuclear phagocytic system (MPS)[9]. As part of the immune system, the cells are primarily macrophages and monocytes. After the systematic administration, the cells immediately sequester the drugs and accumulate in the spleen and lymph nodes[10]. Phagocytosis and opsonization are two categories for such a process.

The foreign proteins with electrostatic and amphiphilic surface induce non-specific interactions like electrostatic, hydrophobic and Van Waals interactions between the serum proteins including serum albumins, apolipoproteins and immunoglobulins in the blood vessel[11-12]. Through specific interactions, proteinaceous molecules can bind to them, which recognizes the specific surface antigenic determinants of exogenous proteins[13]. Opsonization stands for the connection between the exogenous proteins and the antibodies in the bloodstream. The subsequent phagocytosis to remove and digest the foreign proteins is launched since the specialized receptors on the membrane of the phagocytic cells are provided with targets from the attached proteins during the opsonization process[14]. That process leads to the fast removal of protein therapeutics, preventing them from exerting functions in the target site and results in the short circulation[15].

1.2.3. Stability of protein

Encountered with abnormal environments such as high temperature[16], various pH values[17], proteases[18], etc., most proteins would become inactive and show poor stability. Ionic concentration (154mM) and physiological temperature (37^{o}C) in the bloodstream are harsher conditions compared to the ones that can ideally preserve the protein activity and structure. In addition, the shear forces[19] created by the blood flow make exogenous proteins easily attached by

the serum proteins. The collective conditions result in the inactivation of protein functions and misfolding or unfolding of proteins.

In the intracellular environment, the intracellular proteins in the cytoplasm are highly crowded. The intense protein-protein interactions largely reduce protein stability[20]. On the other hand, acidic pH values and excessive proteases in the lysosome and the late endosome lead to dysfunction and fragmentation of proteins, and hydrolysis and proteolysis of the protein sequences[21].

1.3 Strategies for protein delivery

Sophisticated nanocarriers have been developed to circumvent the biological barriers for protein delivery[22,23]. Liposome, similar to cell membranes in structure, exhibit high biocompatibility by encapsulating the drugs in the inner hydrophilic core. However, the shear force created by the blood flow may rupture the assembly of the phospholipids when this kind of nanoscale artificial vesicle is systemically delivered. In addition, liposomes may undergo immune clearance due to recognition by the MPS. To tackle this problem, stealth polymers are incorporated into the structure known as polymersomes. Post-conjugation of polyethylene glycol (PEG) on the liposomes and peg-conjugated lipids are widely adopted techniques. The circulation half-life of polymersomes is increased due to shielding immune recognition originated from the hydrophilic nature of PEG. Oncaspar[24] and Krystexxa[25] are FDA-approved PEGylated therapies for acute lymphoblastic leukemia and hyperglycemia, respectively. After long-term exposure, approximately 30% of patients may develop anti-PEG antibodies[26], which leads to the rapid clearance of the drugs. The inability to degrade the inorganic carriers including mesoporous silica, carbon nanotubes and gold nanoparticles brings safety concerns in the biological systems although there are some extra benefits such as controlled release, imaging contrast and the photothermal

effect. The ideal delivery vehicle should guarantee the stability of the protein and its circulation half-time to realize targeted delivery without any immune responses.

1.3.1. Strategies for intracellular delivery

The nanoparticles should be engineered with various properties to transverse the cell membrane to facilitate intracellular protein therapeutics delivery[27]. One of the most common methods is to design cationic coating on the surface of nanoparticles, which can interact with the negatively charged cell membrane via electrostatic force. This technique shows significant cell membrane permeability and can be achieved using the amine-containing polymers, polypeptides and cationic liposomes[28] while its application is restricted by the poor stability and cytotoxicity[29,30].

Targeting ligands, including aptamers, antibodies and vitamins, are promising candidates[31-33] to enhance cell internalization selectivity since they can bind to receptors or antigens on the surface of the cell membrane when being conjugated to the nanoparticles. In addition, a variety of densities and types of targeting ligands determine the target strength of interactions between cell surface and nanoparticles.

Conjugating cell-penetrating peptides (CPPs), peptides with sequences of no more than 30 amino acids, to the nanoparticles is another approach to address the cell membrane[29]. Several natural sequences such as penetratin[34], transportan[35] and TAT[36,37] have been discovered recently.

1.3.2. Strategies for systematic delivery

The MPS barrier needs to be addressed by the nanoparticles to achieve successful systematic delivery[38], contributing to its long circulation halftime in the plasma. Stealth surface

and neutrally charged properties on the nanoparticles are two current strategies to block the opsonization and evade MPS clearance.

Variety types of low-immunogenic and biocompatible polymers, such as PEG[39], PVP[40] and PHEMA[41] have been utilized in the construction of nanoparticle shells. The "stealth" polymers can help prevent the recognition of the epitope of proteins and serum protein adsorption by the immune system, allowing prolonging circulation time and reducing immunogenicity[42]. For instance, PEG is the most widely used material ,and PEGylation can improve the biodistribution and the pharmacokinetic profiles.

1.4 Protein nanocapsule technology

Our lab has developed and designed a protein nanocapsule technology in light of challenges in intracellular protein delivery[43]. Credit to the in situ polymerization, protein molecules can be encapsulated by the thin polymer shell composed of crosslinkers and monomers. The synthesis process could be achieved in two steps. Due to the surface energy limitation, the protein nanocapsules in the aqueous solution are within the diameter of 25-35 nm in its size while exhibiting spherical morphology regardless of the surface charge and molecular weight of the encapsulated proteins. On the other hand, the surface property is highly tunable and precisely adjusted using different ratios of various monomers and crosslinkers. Meanwhile, the enhanced protein stability can be achieved by the polymer shell interconnected via covalent bonds. Functional groups like -COOH or $-NH_2$ on the monomers enable the protein nanocapsule to be further conjugated by targeting ligands such as antibodies and peptides. Moreover, this technique can also achieve controlled release of the protein payload by incorporating degradable crosslinkers, which can break down in response to protease, pH or light. Furthermore, multi-protein

nanocapsules are proved to provide consecutive catalysis of reactions and higher turnover efficiency by mimicking cellular compartmentalization. In conclusion, this nanocapsule technology is designed for a broad range of therapeutic applications with a large range of versatility and flexibility in molecular synthesis and design.

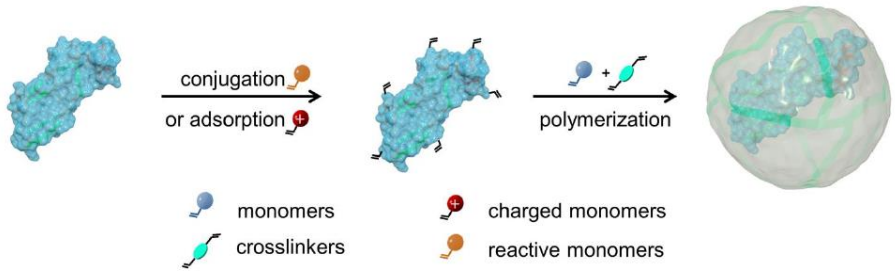

Figure 1-1. Schematic demonstration of the single protein nanocapsules encapsulating the protein molecule by forming crosslinked polymer shell via in situ polymerization[61]. Unsaturated molecules are first absorbed or conjugated to the surface of the protein, followed by the forming of the polymer shell through the launch of free radical polymerization.

1.5 Nanocapsule technology with encapsulated luciferase

As a natural biological process, cell membranes selectively translocate the substances and separate the intracellular space from the extracellular content[44]. Beyond that, great interests have been in biomolecular molecules delivery like genes and proteins into cells for therapy, gene editing and other purposes[45-48]. Since nanoparticular vectors are vital in such intracellular delivery, it is of importance to quantify the internalization kinetics. Essential parameters toward delivery outcomes like cell selectivity, rate of internalization and delivery efficiency can be derived[49, 50].

Fluorescence-activated cell sorting (FACS) and fluorescent microscopy techniques are widely used tools to examine the internalization process[51-54]. However, these two methods only obtain the discrete internalization process at certain time points and pre-treatment steps including rinse, fixation and detachment are required. In addition, fluorescence-based methods to approach the intensity assessment of internalized nanoparticles rely on individual measurement apparatus. Moreover, difficulty in distinguishing the fluorescent signals without extra treatment is another issue. The fluorophores bounding on the cell membrane or within the cells can provide fluorescent signals.

As an oxidative enzyme, firefly luciferase (Fluc) can produce bioluminescence by catalyzing luciferin. There is more sensitivity for luciferase in signaling quantification[55] compared to GFP protein, which guarantees its application including clinical imaging, biology and gene engineering. Moreover, it is ideal for cancer cell detection since bioluminescence requires Mg2+, substance and adenosine-5'-triphosphate (ATP).

Cancer has always attracted great attention among therapeutic, biological and pharmaceutical scientists[56]. Detection is prominent in the prevention of metastasis and diagnosis apart from the development of clinical and therapy methods. Cancerous cells have several characteristics including invasive cell growth, abnormally limitless division, speedy metabolism process and blood vessel construction promotion. Times higher level of ATP concentration than normal cells is a remarkable difference between normal cells and cancerous cells. In this context, luciferase can help find out the ATP-abundance cancerous cells and luciferase encapsulation can be used as a detection method since ATP plays an element role in emitting light signals.

Herein, Our group has reported the real-time nanoparticle internalization kinetics assay (RNICA) based on bioluminescent nanoparticles. As the common phosphate donor in the cells,

ATP has a significant difference crossing the cell membrane, the concentration of which in the extracellular environment (1-1000 nM) is substantially lower than that in the cytosol (1-10 mM)[57, 58]. During the cell internalization process, the bioluminescent reaction in the cells can be promoted by the abrupt increase of the ATP concentration. In this scenario, FLuc is considered as an effective probe for cell internalization with low background and high sensitivity. Di et al[59] has designed and developed a library of Fluc nanoparticles with tunable surface charge and modification moieties including targeting, PEG and cell penetrative ones. Afterwards, the bioluminescence is recorded, which is further converted to real-time kinetics of the nanoparticles. Therefore, FLuc nanoparticles have flexible versatilities and enable fast quantification of the real-time kinetics of nanoparticles.

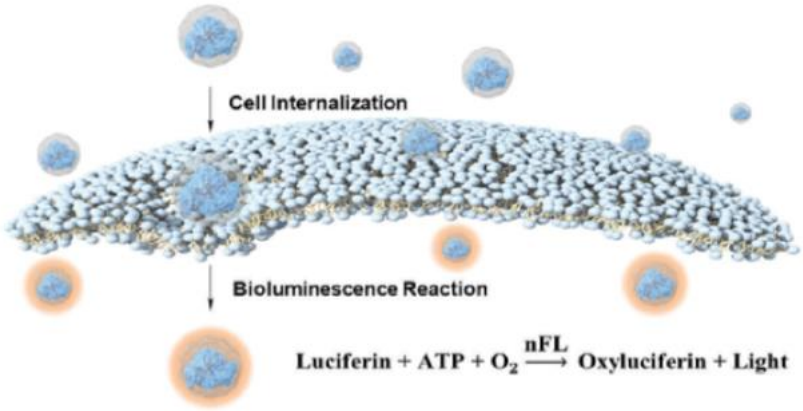

Figure 1-2. Schematic description of the bioluminescent reaction of luciferin catalyzed by the internalized nFLuc in the presence of ATP[59].

In this thesis, the extent of the single-protein delivery system encapsulating firefly luciferase is explored in the field of induced apoptosis in cancer cells. The properties of nFLuc are characterized and in vitro experiments are carried out to examine the cellular internalization.

2 Materials and Methods

2.1 Materials

All materials and chemicals were purchased from Sigma-Aldrich unless were used as received and otherwise noted. LB medium was bought from Genesee Scientific Corporation. Recombinant Escherichia coli (E. coli) expressing Firefly Luciferase was purchased from Excellgen, Inc. The nickel-resin, Hispur^{TM} Ni-NTA, and column was purchased from Thermo Scientific. Luciferin potassium salt were purchased from Gold Biotechnology. Cell Titer Blue cell viability assay kit was purchased from Promega Corporation. HeLa cells were purchased from American Type Culture Collection (ATCC). Fetal Bovine Serum (FBS) was obtained from Corning. Dulbecco's Modified Eagle Medium (DMEM) growth medium, Penicillin-Streptomycin and 0.25% Trypsin were purchased from GenClone. Paclitaxel was obtained from Aladdin Industrial Corporation.

2.2 Instruments

UV-Visible spectra were acquired with a NanoDrop One (Thermo Scientific). Zeta Potential and Dynamic light scattering (DLS) studies of the enzyme nanocomplexes were performed on a Zetasizer Nano (Malvern Instruments Ltd., Kingdom). Transmission electron microscope (TEM) images were obtained on T12 Quick CryoEM and CryoET (FEI). Cells were maintained in a Heracell VIOS 160i CO_2 Incubator (Thermo Scientific). Flow cytometry was performed with a MACSQuant Analyzer (Miltenyi Biotec). The bioluminescence intensities and absorbance were measured with a Tecan Infinite 200 PRO plate reader.

2.3 Production and purification of FLuc

2.3.1. Extraction of crude luciferase

Bacterial cells can produce recombinant Firefly Luciferase. Recombinant *E. Coli* Rosetta2 strain was cultured and the bacteria cells were grown in LB medium (25 g/L) combined with kanamycin (50 g/mL) at 37 °C overnight in a shaking incubator (shaken at 170 rpm) until reaching 0.8 at OD600. Isopropyl-D-thiogalactoside (IPTG) (1 mM) was then added to the medium to achieve the induction of the expression of firefly luciferase. There was a 24-hour induction period and the temperature was kept at 16 °C to protect the enzymatic activity of the FLuc. After induction, the *E. Coli* cells were harvested by centrifugation (5300 rpm) for 10 min and resuspended in Purification Buffer (50 mM NaH_2PO_4, 200 mM NaCl, pH 7.4). An appropriate amount of phenylmethylsulfonyl fluoride (PMSF) (1M) was then added for cell lysis. The FLuc protein was extracted via sonication in intervals for 15 min, centrifugation at 17,000 rpm for 90 min, and passing through a 0.22 μm vacuum filter.

2.3.2. Immobilized metal affinity chromatography using Ni-NTA Resin Column

Ni-NTA resin column was used to achieve the purification of the FLuc from the other proteins. The column. The protein extracts were passed through the column which was first equilibrated with the purification Buffer. The weakly bound contaminating proteins were washed away by 10 column volumes of Purification Buffer and 10 column volumes of each Washing Buffer in ascending order (20 mM, 40 mM, 60 mM imidazole in Purification Buffer). 250 mM imidazole in Purification Buffer was used as the eluant to finally elute the his-tagged Firefly Luciferase. After the enzymatic activity of the elution was monitored, the protein was dialyzed 6 times against PBS for 3 days to remove imidazole. All materials were prechilled at 4 °C to protect

the activity of the protein throughout the purification process. The extracted protein was later stored in aliquots at -80 °C.

2.4 Synthesis of the Firefly Luciferase nanoparticles (nFLuc)

2.4.1. Preparation of the protein nanoparticles

Based on the *in situ* polymerization methods, the proteins FLuc and BSA were encapsulated. Monomer stock solutions for polymerization including N-(3-aminopropyl) methacrylamide (APM) and acrylamide (AAM) were prepared as 20% (m/v) and 30% (m/v) in PBS. Reagents of N, N'-methylene bisacrylamide (BIS) were made as 10% (m/v) in DMSO to crosslink the monomers. Further, magnesium sulfate ($MgSO_4$) and adenosine triphosphate (ATP) were prepared as 100mM in DI water and 50mM in PBS respectively to protect the activity of the FLuc. After dilution by the PBS buffer, The protein concentration of BSA and FLuc became 44 μM in 400μL solution. To start the encapsulation process, the proteins were mixed with a collective solution including AAM, APM, BIS, ATP, $MgSO_4$ first with a ratio listed in table 2-1 along with 220 μL PBS buffer. After gently mix and centrifugation, the polymerization was initiated with 6 μL of ammonium persulfate (APS, 10% in DI water, *m/v*) and catalyzed with 7.9 μL of tetramethylethylenediamine (TEMED) and kept on ice (0-4 ^{o}C) for 1 h. After encapsulation, unreacted reagents would be removed when the solution was dialyzed against prechilled PBS. To determine the encapsulated protein concentration after polymerization and dialysis, BCA Assay was used according to the section above. Encapsulated Firefly Luciferase, herein denoted as nFLuc, was kept on ice until further experimentation. The details of nBSA and nFLuc were listed in Table 2-1.

Table 2-1. Synthesis parameters of nanoparticles

Sample	Protein	AAM	APM	BIS	APS	TEMED	ATP	MgSO4
nFLuc	1	5200	500	500	125	3200	100	100
nBSA	1	5200	500	500	125	3200	100	100

2.4.2. Protein concentration determination

Pierce™ BCA Protein Assay kit was used to determine the protein concentration of protein nanoparticles like nBSA and nFLuc. Native protein BSA were prepared with a series of standard stock in concentrations of 0, 0.5, 1.0, and 2.0 mg/mL. The reacting mixture was prepared by combining BCA Reagent A with BCA Reagent B in a 50:1 ratio. Then, each unknown and standard sample was prepared by mixing 5 μl of the sample with 100 μL of DI water, followed by 100 μL of the reacting mixture containing both BCA Reagent A and B. After the mixture was incubated in a water bath at 60 °C for 30 minutes, 60 μL of each sample in triplicate was then measured under the absorbance at 562 nm. The concentration values of unknown samples were then calculated compared with the standard curves.

2.4.3. Purification method for nanoparticles

One type of the anion exchange column was utilized to purify the nBSA and nFLuc from their unencapsulated counterparts. Since the surface charge of the macromolecule in this platform is increased and proved to be positive due to the thin shell composed of AAM and APM surrounding the protein, the unencapsulated protein is likely to have interactions with the cation stationary phase in the ion exchange column while nanoparticles do not. The sample was prepared by first being transferred to a 20 mM PB dilute buffer and ultracentrifuged at 4000 rpm for 30 min. The sample was then loaded after the ion-exchange column (Q Sepharose Fast Flow, GE Healthcare) was equilibrated with 20 mM PB buffer. Gravity can let the solution flow through.

The elution was monitored under UV light in aliquots and an increasing amount of 20 mM PB was added until the unbound nFLuc were finally eluted. The purified sample was collected and concentrated for further use. To ensure the ion exchange column for future use, the column was washed with 2 column volumes (CVs) of 2M NaCl, 4 CVs of 1M NaOH, another 2 CVs of 2M NaCl, and 2 CVs of DI water in the cleaning step. Afterwards, the column was stored in DI water and kept in the refrigerator at 4 °C until further use.

2.5 Characterization of nFLuc

2.5.1. Preliminary size and charge determination by Agarose Gel Electrophoresis

0.8% (w/v) agarose gel was prepared in TAE buffer (pH 8.3). 10 μL of the samples (~ 1mg/mL) labeled with Fluorescein isothiocyanate (FITC) were added into the wells of the agarose gel. Native protein solution with FITC label served as the control group. The electrophoresis was run at 120mA and 120 V for 12 mins in the Edvoket M12 electrophoresis cell. Afterwards, the agarose gel was examined under UV light. When the experiment is done, the agarose gel would be tossed away and the surface of the instrument should be cleaned with DI water.

2.5.2. Protein purity and encapsulation efficiency examined by SDS-PAGE

SDS-PAGE was utilized to assess the encapsulation efficiency of the nanoparticles. It was carried out in a stacking gel consisting of 4% acrylamide and a separating gel consisting of 10% acrylamide. The samples were mixed with equal volumes of Loading Buffer (100 mM fresh dithiothreitol in 125 mM Tris-Cl, pH 6.8, 2.5% sodium dodecyl sulfate, 25% glycerol, 0.01% *w/v* bromophenol blue). It was then loaded in parallel with a protein ladder as the control in the wells of a freshly fabricated SDS-PAGE. The gel was then run at 45 mA and 300V until the free-dye

indicator ran out of the gel. The fixing buffer (10% *v/v* acetic acid, 50% *v/v* ethanol in DI water) was used to rinse the SDS-PAGE gel for an hour to immobilize the separated proteins. Afterwards, the gel was then placed in the staining buffer (10% *v/v* acetic acid, 50% *v/v* ethanol, 0.5 mg/ml Coomassie Brilliant Blue in DI water) for another one hour. After the excess stain was removed in De-staining Buffer (5% *v/v* acetic acid, 25% *v/v* ethanol in DI water) or deionized water, the pigmented bands indicate the purity and the encapsulation efficiency compared to the known control.

2.5.3. Measurement of particle size and Zeta Potential by dynamic light scattering

Dynamic Light Scattering was used to examine the size distribution and hydrodynamic radius of a sample. In addition, the Zeta Potential can be measured via observation of its electrophoretic. The samples were diluted in 20 mM PB buffer to a concentration of 1 mg/mL. Dry and clean folded capillary cells holding diluted samples were tested for size and surface charge in a Zetasizer Nano ZS (Malvern Co.). The number distribution of nanoparticles was compared to the native proteins.

2.5.4. Transmission Electron Microscopy imaging of nanoparticles

The image captured by the Transmission Electron Microscope was commonly utilized to examine the morphology and size of various nanoparticles. Diluted to a concentration of 0.1 mg/mL, 2 μL nanocapsule solution was dipped on a carbon-coated copper grid. After contacting the grids for 1 min, the excess amount of sample was removed by filter papers. The grid was then stained with uranium acetate (2% w/v) and incubated for another 1.5 mins. The grid was left

overnight after the uranium acetate was removed. Once the grid was getting dried out, it was inspected under TEM.

2.5.5. Enzymatic activity assay for nanoparticles

The activities of FLuc nanoparticles and native FLuc were quantified by monitoring the bioluminescence reaction rate. The Substrate Buffer was prepared to consist of 3.74 mM magnesium sulfate ($MgSO_4$), 20 mM tricine, 2 mM dithiothreitol (DTT) and 0.1 mM ethylenediaminetetraacetic acid (EDTA) in DI water, followed by adjusting the pH to 7.4. Other stock solutions, such as ATP (50mM in PBS), Luciferin (10mM in PBS), and Coenzyme A (CoA, 10mM in DI water) were made. The 915.5 μL of Substrate Buffer was then supplemented with 10.6 μL ATP solution, 47 μL luciferin solution and 27 μL of CoA solution to prepare the activity buffer. 2 μL of the nFLuc or native FLuc sample (2.5 mg/mL) were then added to 35 μL of activity buffer in a 96-well plate to perform the activity assay. The bioluminescent intensity was quickly monitored with an exposure time of 1 second using a plate reader. The enzymatic activities comparison between the native FLuc and nFLuc can be analyzed based on the bioluminescence reaction rate test.

2.5.6. Proteolytic and Thermal Stability assays of nFLuc and FLuc

The proteolytic and thermal stability of nFLuc and native FLuc were assessed to monitor the activity of enzymes incubated with protease and PBS at 37 ^{o}C. For the proteolytic stability test, The HeLa cells (10^5 cells) were rinsed and aspirated with PBS buffer. In detail, the samples (0.4 mg/mL nFLuc or native FLuc) were added to warmed PBS. The samples were then added to a protease solution (0.1% Trypsin-EDTA in PBS). Over 45 minutes the residual activity of the

samples was measured. The thermal stabilities were monitored in PBS at 37 °C. The ability was observed based on similar sample incubation methods. The activity of the sample was also measured over 45 minutes.

2.6 In vitro treatment and assay

2.6.1. Cell culture method

HeLa cell lines were purchased from American Type Culture Collection (ATCC). HeLa cells were maintained and grown in Dulbecco's Modified Eagle Medium (DMEM), supplemented with 1% penicillin/ streptomycin (P/S) and 10% fetal bovine serum (FBS) in an atmosphere of 5% carbon dioxide at 37 °C. The subculture protocol follows the recommended protocol of ATCC. In detail, the serum with trypsin inhibitor can be removed by rinsing the HeLa cells with PBS buffer. 1mL trypsin-EDTA solution addition and incubation for about 2 mins at 37 ^{o}C can achieve trypsinization when the cells detached. After the cell layer was detached, 4mL DMEM medium with 1% P/S and 10% FBS was utilized to stop the trypsinization. After centrifugation, an appropriate ratio of the 1mL cell suspension was added to the new cell culture flask.

2.6.2. In vitro Cellular penetrability (fluorescent-activated cell sorting test)

Fluorescent-activated cell sorting (FACS) test was used to assess the cell internalization kinetics of nFLuc. The labeling reagent FITC (1% w/v in DMSO) was conjugated to APM monomers in the polymer shell of nFLuc in a 3:1 FITC to nFLuc ratio to prepare nFLuc for being detected in the flow cytometry. After the pH was adjusted by sodium bicarbonate buffer (100mM) to 8.0, the reaction was protected from the light and sit for 1 h. Any unconjugated labeling reagent would be removed by dialysis in PBS 2 times. BCA Assay was conducted to examine the

concentration of the protein in the sample, which would then be stored in a 4 °C refrigerator until further use.

HeLa cells (~10^4 cells per well) were seeded in a 96-well plate. After the cells properly adhere to the plate overnight, They were then treated with nFLuc for designed incubation times. The medium was aspirated and the cells were gently rinsed with PBS after the desired exposure to nFLuc to remove any remaining serum proteins and nFLuc. The cells were then treated with trypsin (0.25% Trypsin-EDTA) in each well, resuspended in DMEM medium with 1% P/S and 10% FBS, and fixed in paraformaldehyde (2.5% Formalin). The fixed cells were then stored in a 4 °C refridgerator overnight until further analysis by the flow cytometer.

The 488 nm laser was used at appropriate voltages to assess the fluorescent intensity of nFLuc inside each cell. A typical dye (0.095% *w/v* Trypan Blue) was used to quench the intensity of any nFL on the exterior of the cellular membrane to make sure fluorescent intensities were mostly contributed from the internalized nFLuc. The forward scatter height (FSC-H) and forward scatter area (FSC-A) charts were scanned for singlets at the beginning of the analysis. Gates based on side scatter area (SSC-A) and critical forward scatter area (FSC-A) was utilized to select the intensities of the cells of concern from the cellular debris. Median Fluorescent Intensities (MFI) and Fluorescent Intensity Histograms values of the nFLuc conjugated by FITC were then extracted using FlowJo whereas PRISM is utilized to analyze the comparison in MFIs.

2.6.3. In-Vitro drug treatment

To monitor the endocytic process in apoptotic cells, cellular apoptosis was induced when HeLa cells were treated with chemotherapeutic treatment applying a variety of concentrations of doxorubicin (0, 0.5, 1, 5, 20 μM in DMEM medium with 1% P/S and 10% FBS) or paclitaxel (0,

2, 5, 20, 100, 2000 nM in DMEM medium with 1% P/S and 10% FBS). The concentrated stock solution was made by dissolving doxorubicin or paclitaxel in dimethyl sulfoxide (DMSO). After dilution in DMEM medium with 1% P/S and 10% FBS, the highest working concentration of DMSO could not exceed 0.1% (*v/v*), which meant no observable toxic effects to cells by DMSO.

The Cell Titer Blue assay was conducted to determine the toxicity of the drug. After desired treatment exposure, the medium with gradient drug concentration was aspirated and replaced with a fresh DMEM medium with 1% P/S and 10% FBS. Each well was incubated with Cell Titer Blue (0.025 mg/mL in DMEM medium with 1% P/S and 10% FBS) for one hour at 37 °C to allow the conversion of the substrate. The fluorescence was then measured using a Tecan Infinite 200 PRO plate reader at an emission wavelength of 590 nm and an excitation wavelength of 560 nm. Control wells were treated with an equal volume of PBS in place of the anticancer drug.

2.7 Kinetic measurements of cell internalization via bioluminescence

Tecan Infinite 200 PRO plate reader was used to keep track of the continuous luminescence intensity of every single well of a 96-well plate for 3 hours to obtain the record of bioluminescence kinetics of cell internalization. In detail, 2×10^4 HeLa cells were seeded into each well and cultured in 100 μL DMEM medium with 1% P/S and 10% FBS for one day. Then, the cell medium was aspired and the cells were rinsed with PBS buffer, and incubated with 100 μL kinetics-test medium (DMEM medium without phenol red with 1% P/S and 10% FBS) carrying desired treatment of paclitaxel for 24h at 37 °C. The Hela cells were added with luciferin (0.5 mg/mL in DMEM medium with 1% P/S and 10% FBS) at the time of drug incubation since the excited state of oxyluciferin is needed to produce light during the bioluminescent reaction. After 24 h, the nFLuc samples were incubated at a final concentration of 0.4 mg/mL in every well and 25 μL of resazurin

(0.15 mg/mL in PBS) was added to the wells in between to block the luminescence. The exposure time was set as 1 second with an interval time of 30 seconds. The moment adding nFLuc samples until the first measurement by the plate reader was timed using a stopwatch.

It is of vital importance to record the number of HeLa cells per well in the real-time measurement in obtaining the quantified amount of nFLuc internalized and monitoring the endocytic process. Another cell plate was prepared and treated in parallel to count the number of cells per well accurately apart from the cell plate for the previous endocytic monitoring assay. The anticancer drug treatment medium in the parallel plate was aspired, gently rinsed with PBS, trypsinized, and fixed in 1% paraformaldehyde overnight at 4 °C. The number of the cells was then counted using the flow cytometer on the other day.

2.8 Quantitative Modeling and Real-Time Endocytic Monitoring using nFLuc

2.8.1. Quantitative Modeling of the cell internalization kinetics

Bioluminescence produced from every single well of the 96 well plates per second was measured to quantify the internalization process. The following equation model (2-1) illustrated the relationship between the recorded bioluminescence (RLU) and the concentration of nFLuc in a cell over time.

$$RLU = \frac{k_{\mathrm{cat}}[S]}{K_{\mathrm{M}}+[S]}[\mathrm{n}FLuc]\mathrm{e}^{-k_{\mathrm{d}}\mathrm{t}} \cdot A \cdot N \qquad (2\text{-}1)$$

Where RLU is the bioluminescent reaction rate with the unit of relative light units per second (RLU/s), k_d is the calculated decay constant of nFLuc, A is the emitted RLUs per mole of luciferin reacted, N is the number of cells per well.

2.8.2. Two Enzymatic Characteristics regarding k_{cat} and K_M

The turnover number (k_{cat}) and the Michaelis constant (K_M) were essential in modeling the temporal bioluminescent rate and were measured via a Lineweaver-Burk plot. Similar to the protocol making activity buffer mentioned in 2.5.5, ATP (10.6 μL, 50 mM in PBS) and Coenzyme A (27 μL, 10 mM CoA in DI Water) were added to Substrate Buffer (915.5 μL). a series of activity buffers were prepared for analysis through adding 47 μL of gradient concentrations of Luciferin (0.625, 1.25, 2.5 5, 10 mM D-luciferin in PBS). 2 μL of nFLuc were then added to 35 μL of the activity buffers and the activity of nFLuc was then recorded at each concentration of Luciferin. A Lineweaver-Burk plot was then graphed using the reciprocal Luciferin-substrate concentration and the corresponding reciprocal bioluminescent rate. K_M and k_{cat} can be finally determined since the y-intercept is $\frac{1}{k_{cat}\cdot[E]}$, where [E] stands for the total enzyme concentration while the x-intercept is $-\frac{1}{K_M}$.

2.8.3. The substrate concentration [S]

The relationship between the change of substrate concentration and the reaction rate of bioluminescence reaction can be described as,

$$r = \frac{\mathrm{d}[S_{in}]}{\mathrm{dt}} = RLU \cdot \frac{1}{A \cdot N} \tag{2-2}$$

$$\Delta[S_{in}] = \int_{t_0}^{t_\infty} r dt = \int_{t_0}^{t_\infty} RLU \cdot \frac{1}{A \cdot N}\, dt \tag{2-3}$$

The initial concentration $[S_{in}]_0$ (2 nM) was largely higher than the concentration change (within the range of 1-20 nM) during the cellular uptake process[59]. Thus, $[S_{in}]_0$ can represent the substrate concentration profile inside the cell. Therefore, the equation regarding the reaction rate can be transformed as,

$$RLU = \frac{k_{\mathrm{cat}} \cdot [S_{in}]_0}{K_{\mathrm{M}} + [S_{in}]_0} \cdot [\mathrm{n}FLuc] \cdot \mathrm{e}^{-K_{\mathrm{d}}\mathrm{t}} \cdot A \cdot N \quad (2\text{-}4)$$

2.8.4. The conversion factor *A*

Since the signals in lysed cells are 68.422 times greater than that obtained from living cells, the value for A was 5.70 x 10^9 RLU/ (mol oxyluciferin)[60] since the conversion factor was determined to be 3.90 x 10^{11} RLU/ (mol oxyluciferin) in the non-cells condition.

2.8.5. The decay constant K_{d}

The equation (2-4) can be presented as,

$$In\ RLU = \mathrm{In}\{\frac{k_{\mathrm{cat}} \cdot [S_{in}]_0}{K_{\mathrm{M}} + [S_{in}]_0} \cdot [\mathrm{n}FLuc] \cdot A \cdot N\} - K_{\mathrm{d}}\mathrm{t} \quad (2\text{-}5)$$

This shows that during the cell internalization process, -K_{d} is the slope of In *RLU* versus time function when the plateau is achieved. In other words, the decay constant can be calculated through the extraction of the line segment using standard Hough transform. Consequently, the concentration of the nanoparticles can be derived from,

$$[\mathrm{n}FLuc] = \frac{RLU}{\frac{k_{\mathrm{cat}} \cdot [S_{in}]_0}{K_{\mathrm{M}} + [S_{in}]_0} \mathrm{e}^{-K_{\mathrm{d}}\mathrm{t}} \cdot A \cdot N} \quad (2\text{-}6)$$

2.8.6. Plateau concentration

Monitoring the standard deviation of the temporal profile of nFLuc concentration can obtain the plateau concentration ([$\mathrm{nFL}_{\mathrm{plateau}}$]). The corresponding index to the plateau concentration was determined when the standard deviation of five adjacent points fell less than 10% of the standard deviation that is of the maximum report.

2.8.7. Initial rate of uptake

The beginning linear portion of the nFLuc concentration curve was selected and analyzed to calculate the initial rate of uptake (IRU). When the squares of correlation met the required values, the slope subject to the linear fit was determined as the IRU.

3 Results and Discussion

3.1 Preliminary charge results

The formation of nFLuc was preliminarily determined by the charge difference of nanoparticles using agarose gel electrophoresis. Nanoparticles and proteins can be separated by size and charge by electrophoresis, which has normal application in separating RNA or DNA segments. Figure 3-1 shows the separation of nFLuc and native FLuc.

The nFLuc sample migrated toward the cathode slightly with hardly observed movement which indicated that the native FLuc was encapsulated successfully and the nanocapsules had higher molecular weight compared to the relatively lower molecular weight and large negative charge of the native protein. The encapsulation of FLuc was successful reconfirmed by the SDS-PAGE where native FLuc migrated to the separating gel and nFLuc remained in the stacking gel.

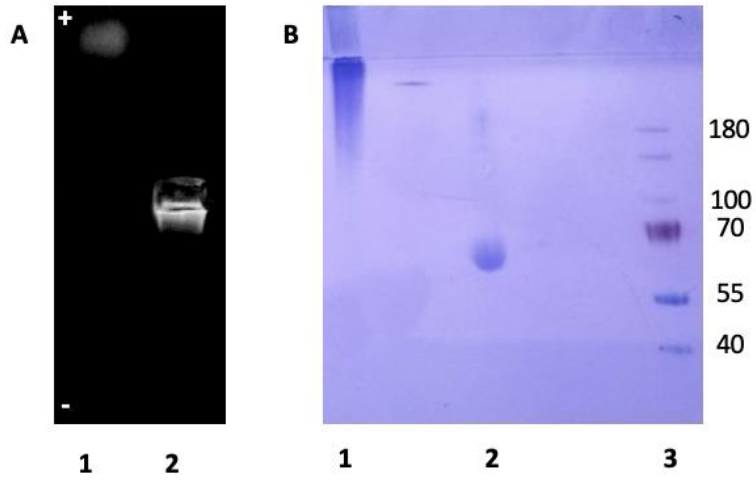

Figure 3-1. Preliminary charge results by agarose gel electrophoresis and SDS-PAGE. A) Agarose gel electrophoresis of 1, native FLuc; 2, nFLuc. B) SDS-PAGE of 1, native FLuc; 2, nFLuc; 3, ladder.

3.2 Particle size and zeta potential of nFLuc

The Zetasizer Nano ZS applied dynamic light scattering (DLS) to further verify the particle size and surface charge of nanoparticles. Moving under Brownian motion, the diffusion of particles can be measured by the analyzer. The signal can then be converted to charge and size distribution using the Stokes-Einstein equation.

In Figure 2, compared to its native counterparts (- 4.55 mV), the nFLuc exhibits a slightly positive potential (+ 3.56 mV). The zeta potential increases linearly corresponding to the ratio of the positive monomer (APM) versus the total amount of monomer (AAM+APM). The surface charge can be tuned to make it possible to engineer the nanoparticle surface for a variety of applications. On the other hand, the hydrodynamic size of the nFLuc was increased from 10.2 nm to 25.1 nm, which results from the polymer shell surrounding the single protein through in situ polymerization. Different components and ratios of incorporated monomers can also adjust the particle size of nanocapsules.

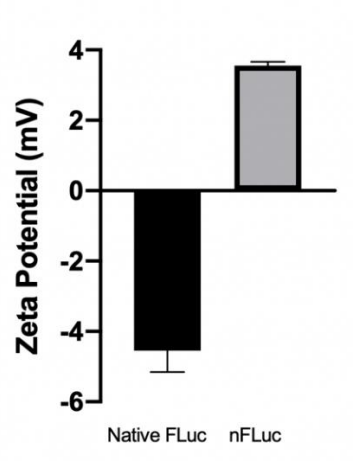

Figure 3-2. Zeta potential distribution of the native Fluc and nFLuc nanoparticles. Mean ± SEM, n=3.

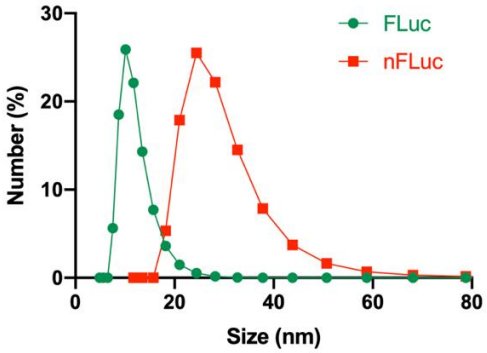

Figure 3-3. Size distribution of the native Fluc and nFLuc nanoparticles.

3.3 TEM imaging of nanoparticles

High-resolution images of nanoparticles can be captured via transmission electron microscopy (TEM). Owing to the de Broglie wavelength of electrons, the TEM technique can examine the intricate detail of particles.

In Figure 4, the consistency of identical spherical morphology of the nFLuc has been observed. Compared to the scale range, the size distribution in diameter is 26.03 ± 0.43 nm, which proves the formulation of the core-shell structure of the single protein nanocapsules.

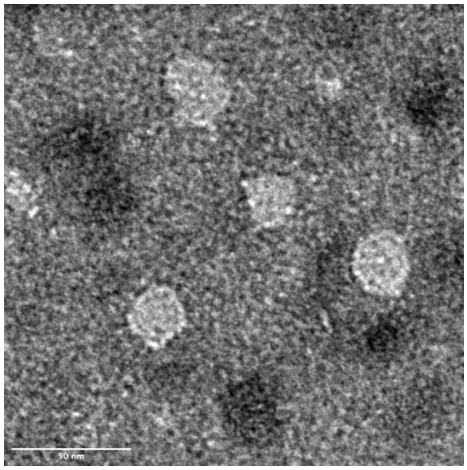

Figure 3-4. TEM imaging of nFLuc nanoparticles showing uniform and spherical morphology.

3.4 Accumulation of nFLuc in Apoptotic Cells induced by paclitaxel and doxorubicin

Apoptosis is a kind of programmed cell death when induced or natural stresses occur. Two types of drug treatments including paclitaxel and doxorubicin have been selected to induce cell apoptosis in which the nFLuc was assessed during the endocytic process. Treated with various concentrations of doxorubicin and paclitaxel, the HeLa cells were then incubated with the nFLuc for an hour. With the increasing concentration of both drug treatments, the distribution shifts of the nanoparticles in terms of intensity can be observed as is shown in Figures 5A and 5B. In Figures 5C and 5D, The median fluorescent intensity (MFI) increased with increasing paclitaxel concentration while it showed no significant difference with a variety of concentrations of doxorubicin treatment，which partly results from the different mechanisms of two anticancer treatments in inducing cellular apoptosis. Using palbociclib, a CDK4/6 inhibitor, to handle the breast cancer cells may provide more detailed and profound information.

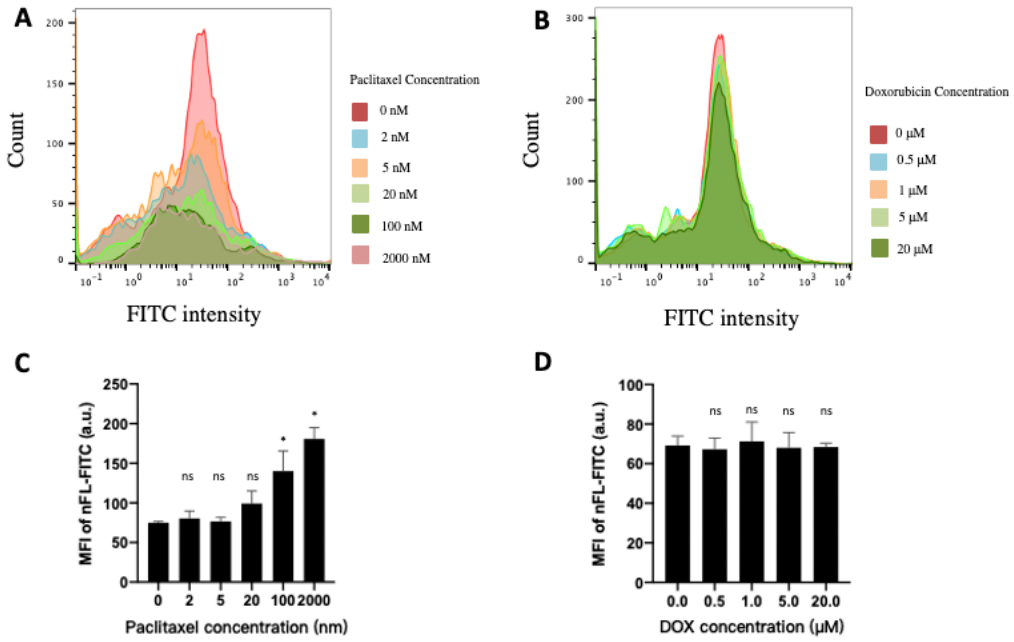

Figure 3-5. Accumulation of nFLuc during cell apoptosis. A) Fluorescence-assisted cell sorting of HeLa cells after paclitaxel treatment with 1 h nFLuc incubation at 37ºC. B) Fluorescence-assisted cell sorting of HeLa cells after doxorubicin treatment with 1 h nFLuc incubation at 37 ºC. C) Median fluorescent intensities (MFI) of HeLa cells treated with various concentrations of paclitaxel and 1 h nFLuc incubation at 37 ºC. D) Median fluorescent intensities (MFI) of HeLa cells treated with various concentrations of doxorubicin and 1 h nFLuc incubation at 37 ºC.

4 Conclusion

The cationic nFLuc nanocapsule was formulated and fabricated. Basic characteristics including surface charge, particle size and morphology have been determined via gel electrophoresis, DLS and TEM imaging. The nanocapsule also shows its unique performance during the cell apoptosis process. The results of distinct bioluminescent rate and the accumulation of nFLuc tell the differences in cellular endocytic processes. High fluorescent intensities were indicated with increasing apoptosis cells induced by paclitaxel. However, it shows no significant difference in other anticancer treatments like incubation with doxorubicin. The technique can be further explored in telling more theoretical differences in a variety of drug treatments and also in the field of cancer versus non-cancer cell lines.

5 References

1. Leader, B., Baca, Q. J., & Golan, D. E. (2008). Protein therapeutics: a summary and pharmacological classification. Nature reviews Drug discovery, 7(1), 21-39.
2. Usmani, S. S., Bedi, G., Samuel, J. S., Singh, S., Kalra, S., Kumar, P., ... & Raghava, G. P. (2017). THPdb: Database of FDA-approved peptide and protein therapeutics. PloS one, 12(7), e0181748.
3. Heath, J. R. (2015). Nanotechnologies for biomedical science and translational medicine. Proceedings of the National Academy of Sciences, 112(47), 14436-14443.
4. Edidin, M. (2003). Lipids on the frontier: a century of cell-membrane bilayers. Nature Reviews Molecular Cell Biology, 4(5), 414-418.
5. Del Vecchio, P. J., Siflinger-Birnboim, A., Shepard, J. M., Bizios, R., Cooper, J. A., & Malik, A. B. (1987). Endothelial monolayer permeability to macromolecules. Federation proceedings, 46(8), 2511–2515.
6. Gruenberg, J., & Maxfield, F. R. (1995). Membrane transport in the endocytic pathway. Current opinion in cell biology, 7(4), 552-563.
7. Huotari, J., & Helenius, A. (2011). Endosome maturation. The EMBO journal, 30(17), 3481-3500.
8. Oh, N., & Park, J. H. (2014). Endocytosis and exocytosis of nanoparticles in mammalian cells. International journal of nanomedicine, 9 Suppl 1(Suppl 1), 51–63.
9. Lasser A. (1983). The mononuclear phagocytic system: a review. Human pathology, 14(2), 108–126.

10. Hume, D. A., Ross, I. L., Himes, S. R., Sasmono, R. T., Wells, C. A., & Ravasi, T. (2002). The mononuclear phagocyte system revisited. Journal of leukocyte biology, 72(4), 621–627.
11. Sarma, J. V., & Ward, P. A. (2011). The complement system. Cell and tissue research, 343(1), 227–235.
12. Frank, M. M., & Fries, L. F. (1991). The role of complement in inflammation and phagocytosis. Immunology today, 12(9), 322–326.
13. Leserman, L. D., Weinstein, J. N., Blumenthal, R., & Terry, W. D. (1980). Receptor-mediated endocytosis of antibody-opsonized liposomes by tumor cells. Proceedings of the National Academy of Sciences of the United States of America, 77(7), 4089–4093.
14. Aderem, A., & Underhill, D. M. (1999). Mechanisms of phagocytosis in macrophages. Annual review of immunology, 17(1), 593-623.
15. Flannagan, R. S., Jaumouillé, V., & Grinstein, S. (2012). The cell biology of phagocytosis. Annual review of pathology, 7, 61–98.
16. Tang, K. E., & Dill, K. A. (1998). Native protein fluctuations: the conformational-motion temperature and the inverse correlation of protein flexibility with protein stability. Journal of Biomolecular Structure and Dynamics, 16(2), 397-411.
17. Yang, A. S., & Honig, B. (1993). On the pH dependence of protein stability. Journal of molecular biology, 231(2), 459-474.
18. Park, C. and Marqusee, S. (2006), Quantitative Determination of Protein Stability and Ligand Binding by Pulse Proteolysis. Current Protocols in Protein Science, 46: 20.11.1-20.11.14.

19. Jaspe, J., & Hagen, S. J. (2006). Do protein molecules unfold in a simple shear flow?. Biophysical journal, 91(9), 3415-3424.
20. Harada, R., Sugita, Y., & Feig, M. (2012). Protein crowding affects hydration structure and dynamics. Journal of the American Chemical Society, 134(10), 4842–4849.
21. Ciechanover A. (2005). Proteolysis: from the lysosome to ubiquitin and the proteasome. Nature reviews. Molecular cell biology, 6(1), 79–87.
22. Liu, Y., Li, J., & Lu, Y. (2015). Enzyme therapeutics for systemic detoxification. Advanced drug delivery reviews, 90, 24–39.
23. Du, J., Jin, J., Yan, M., & Lu, Y. (2012). Synthetic nanocarriers for intracellular protein delivery. Current drug metabolism, 13(1), 82–92.
24. Dinndorf, P. A., Gootenberg, J., Cohen, M. H., Keegan, P., & Pazdur, R. (2007). FDA drug approval summary: pegaspargase (oncaspar) for the first-line treatment of children with acute lymphoblastic leukemia (ALL). The oncologist, 12(8), 991–998.
25. Schlesinger, N., Yasothan, U., & Kirkpatrick, P. (2011). Pegloticase. Nature reviews. Drug discovery, 10(1), 17–18.
26. Longo, N., Harding, C. O., Burton, B. K., Grange, D. K., Vockley, J., Wasserstein, M., Rice, G. M., Dorenbaum, A., Neuenburg, J. K., Musson, D. G., Gu, Z., & Sile, S. (2014). Single-dose, subcutaneous recombinant phenylalanine ammonia lyase conjugated with polyethylene glycol in adult patients with phenylketonuria: an open-label, multicentre, phase 1 dose-escalation trial. Lancet (London, England), 384(9937), 37–44.
27. Chou, L. Y., Ming, K., & Chan, W. C. (2011). Strategies for the intracellular delivery of nanoparticles. Chemical Society Reviews, 40(1), 233-245.

28. Leroueil, P. R., Hong, S., Mecke, A., Baker, J. R., Jr, Orr, B. G., & Banaszak Holl, M. M. (2007). Nanoparticle interaction with biological membranes: does nanotechnology present a Janus face?. Accounts of chemical research, 40(5), 335–342.

29. Chatterjee, D. K., Rufaihah, A. J., & Zhang, Y. (2008). Upconversion fluorescence imaging of cells and small animals using lanthanide doped nanocrystals. Biomaterials, 29(7), 937–943.

30. Herrero, M. A., Toma, F. M., Al-Jamal, K. T., Kostarelos, K., Bianco, A., Da Ros, T., Bano, F., Casalis, L., Scoles, G., & Prato, M. (2009). Synthesis and characterization of a carbon nanotube-dendron series for efficient siRNA delivery. Journal of the American Chemical Society, 131(28), 9843–9848.

31. Rajendran, L., Knölker, H. J., & Simons, K. (2010). Subcellular targeting strategies for drug design and delivery. Nature reviews. Drug discovery, 9(1), 29–42.

32. Bareford, L. M., & Swaan, P. W. (2007). Endocytic mechanisms for targeted drug delivery. Advanced drug delivery reviews, 59(8), 748-758.

33. Torchilin V. P. (2006). Recent approaches to intracellular delivery of drugs and DNA and organelle targeting. Annual review of biomedical engineering, 8, 343–375.

34. Derossi, D., Chassaing, G., & Prochiantz, A. (1998). Trojan peptides: the penetratin system for intracellular delivery. Trends in cell biology, 8(2), 84–87.

35. Gupta, B., Levchenko, T. S., & Torchilin, V. P. (2005). Intracellular delivery of large molecules and small particles by cell-penetrating proteins and peptides. Advanced drug delivery reviews, 57(4), 637–651.

36. Torchilin V. P. (2008). Tat peptide-mediated intracellular delivery of pharmaceutical nanocarriers. Advanced drug delivery reviews, 60(4-5), 548–558.

37. Torchilin, V. P., Rammohan, R., Weissig, V., & Levchenko, T. S. (2001). TAT peptide on the surface of liposomes affords their efficient intracellular delivery even at low temperature and in the presence of metabolic inhibitors. Proceedings of the National Academy of Sciences of the United States of America, 98(15), 8786–8791.
38. Pisal, D. S., Kosloski, M. P., & Balu-Iyer, S. V. (2010). Delivery of therapeutic proteins. Journal of pharmaceutical sciences, 99(6), 2557-2575.
39. Harris, J. M., & Chess, R. B. (2003). Effect of pegylation on pharmaceuticals. Nature reviews. Drug discovery, 2(3), 214–221.
40. Gallardo, A., Rocío Lemus, A., San Román, J., Cifuentes, A., & Díez-Masa, J. C. (1999). Micellar electrokinetic chromatography applied to copolymer systems with heterogeneous distribution. Macromolecules, 32(3), 610-617.
41. Liu, H., Chen, Y., Shen, Z., & Frey, H. (2007). Multiarm star polyglycerol-block-poly (HEMA) as a versatile precursor for the preparation of micellar nanocapsules with different properties. Reactive and Functional Polymers, 67(2), 156-164.
42. Amoozgar, Z., & Yeo, Y. (2012). Recent advances in stealth coating of nanoparticle drug delivery systems. Wiley interdisciplinary reviews. Nanomedicine and nanobiotechnology, 4(2), 219–233.
43. Yan, M., Du, J., Gu, Z., Liang, M., Hu, Y., Zhang, W., Priceman, S., Wu, L., Zhou, Z. H., Liu, Z., Segura, T., Tang, Y., & Lu, Y. (2010). A novel intracellular protein delivery platform based on single-protein nanocapsules. Nature nanotechnology, 5(1), 48–53.
44. Stewart, M. P., Sharei, A., Ding, X., Sahay, G., Langer, R., & Jensen, K. F. (2016). In vitro and ex vivo strategies for intracellular delivery. Nature, 538(7624), 183–192.

45. Papapetrou, E. P., Tomishima, M. J., Chambers, S. M., Mica, Y., Reed, E., Menon, J., Tabar, V., Mo, Q., Studer, L., & Sadelain, M. (2009). Stoichiometric and temporal requirements of Oct4, Sox2, Klf4, and c-Myc expression for efficient human iPSC induction and differentiation. Proceedings of the National Academy of Sciences of the United States of America, 106(31), 12759–12764.
46. Gratton, S. E., Ropp, P. A., Pohlhaus, P. D., Luft, J. C., Madden, V. J., Napier, M. E., & DeSimone, J. M. (2008). The effect of particle design on cellular internalization pathways. Proceedings of the National Academy of Sciences of the United States of America, 105(33), 11613–11618.
47. Verma, A., & Stellacci, F. (2010). Effect of surface properties on nanoparticle-cell interactions. Small (Weinheim an der Bergstrasse, Germany), 6(1), 12–21.
48. Torchilin V. (2008). Intracellular delivery of protein and peptide therapeutics. Drug discovery today. Technologies, 5(2-3), e95–e103.
49. Teeguarden, J. G., Hinderliter, P. M., Orr, G., Thrall, B. D., & Pounds, J. G. (2007). Particokinetics in vitro: dosimetry considerations for in vitro nanoparticle toxicity assessments. Toxicological sciences : an official journal of the Society of Toxicology, 95(2), 300–312.
50. Kamiya, H., Akita, H., & Harashima, H. (2003). Pharmacokinetic and pharmacodynamic considerations in gene therapy. Drug discovery today, 8(21), 990–996.
51. Watson, P., Jones, A. T., & Stephens, D. J. (2005). Intracellular trafficking pathways and drug delivery: fluorescence imaging of living and fixed cells. Advanced drug delivery reviews, 57(1), 43–61.

52. Stephens DJ, Allan VJ. Light microscopy techniques for live cell imaging. Science. 2003 Apr 4;300(5616):82-6.

53. Gregersen, K. A., Hill, Z. B., Gadd, J. C., Fujimoto, B. S., Maly, D. J., & Chiu, D. T. (2010). Intracellular delivery of bioactive molecules using light-addressable nanocapsules. ACS nano, 4(12), 7603–7611.

54. Lippincott-Schwartz, J., & Patterson, G. H. (2003). Development and use of fluorescent protein markers in living cells. Science (New York, N.Y.), 300(5616), 87–91.

55. Choy, G., O'Connor, S., Diehn, F. E., Costouros, N., Alexander, H. R., Choyke, P., & Libutti, S. K. (2003). Comparison of noninvasive fluorescent and bioluminescent small animal optical imaging. BioTechniques, 35(5), 1022–1030.

56. Nogawa, M., Yuasa, T., Kimura, S., Kuroda, J., Sato, K., Segawa, H., Yokota, A., & Maekawa, T. (2005). Monitoring luciferase-labeled cancer cell growth and metastasis in different in vivo models. Cancer letters, 217(2), 243–253.

57. Morciano G, Sarti AC, Marchi S, Missiroli S, Falzoni S, Raffaghello L, Pistoia V, Giorgi C, Di Virgilio F, Pinton P. Use of luciferase probes to measure ATP in living cells and animals. Nat Protoc. 2017 Aug;12(8):1542-1562.

58. Mo, R., Jiang, T., Sun, W., & Gu, Z. (2015). ATP-responsive DNA-graphene hybrid nanoaggregates for anticancer drug delivery. Biomaterials, 50, 67–74.

59. Wu, D., Yang, Y., Xu, P., Xu, D., Liu, Y., Castillo, R., ... & Lu, Y. (2019). Real-Time Quantification of Cell Internalization Kinetics by Functionalized Bioluminescent Nanoprobes. Advanced Materials, 31(39), 1902469.

60. Ignowski, J. M., & Schaffer, D. V. (2004). Kinetic analysis and modeling of firefly luciferase as a quantitative reporter gene in live mammalian cells. Biotechnology and bioengineering, 86(7), 827–834.
61. Liu, Y., Li, J., & Lu, Y. (2015). Enzyme therapeutics for systemic detoxification. Advanced drug delivery reviews, 90, 24-39.